A semisynthetic peptide-metalloporphyrin responsive matrix for artificial photosynthesis

Sun, Z.

Chapter 3

Contrasting modes of modulated self-assembly for CsmA homologues coordinated to ZnPP

3.0 Abstract

The self-assembly of different homologues of tCsmA with ZnPP is studied. The results indicate that the high pH of dialysis buffer, the net charge, and α-helical structure of the peptide and the binding of ligand are important for the self-assembly. The tCsmA and ZnPP form two different modes of modulated self-assembly. The major type shows a 7_2 helical structure. When dialyzing the 7_2 helical assembly from the KPi buffer to the Tris buffer, a para-crystalline sheet similar to the natural baseplate can be observed by cryo-EM, showing that changing buffer can lead to a different structure. The para-crystalline sheets can be established by the untwisting of the helical structure and the formation of salt bridges between antiparallel peptide strands with arrays of dimeric ZnPP coordinated to the histidyl between the strands. In contrast, in the helical filaments the polar residues are solvent exposed on the outside of the 7_2 helix, and the self-assembly is stabilized predominantly by dipole-dipole interactions for chromophores and helices in the Tris buffer.

Zhongwu Sun, Christoph A. Diebolder, Ludovic Renault, Huub de Groot. Contrasting modes of modulated self-assembly for truncated CsmA and ZnPP, *To be submitted*

3.1 Introduction

As the smallest photosynthetic antenna known in nature, the CsmA-BChl *a* complex from the baseplate of *Chlorobaculum tepidum* is of interest for the design of semisynthetic building blocks for light harvesting in artificial photosynthesis.[1] The system assists in energy transfer and storage from the chlorosome to the FMO antenna and the photosynthetic reaction center.[2] The 59-residue CsmA protein is predominantly α-helical. It includes a long helical domain extending over residues 6–36, and a short helix in the C-terminal part formed by residues 41–49. Two flexible segments in both terminals attach to the chlorosome and the FMO antenna, respectively.[3] The BChl *a* coordinates to the His 25. CsmA is an amphipathic peptide. Except for the single coordinating histidine on the hydrophobic side, all potentially charged residues, like lysine and arginine, are located at the hydrophilic side of the helix.[4-6] Antiparallel dimers of CsmA-BChl *a* self-assemble to form extended para-crystalline layers with BChl *a* in between two CsmA strands running in opposite directions, bound to the next pair of strands by salt bridges.[7-8]

α-Helical peptides are often used as building blocks for self-assembly. In this chapter, I prepare different homologues of the natural CsmA by removing flexible segments from the N and C-terminals (Table 3.1). This leaves the functional central α-helix as the peptide motif to bind zinc-protoporphyrin (ZnPP) and form a semisynthetic scaffold. The semisynthetic tCsmA construct that is also used in the previous chapter contains 43 amino acids and is capped at the C-terminus with acetate and at the N-terminus with amine. In the F-CsmA, both caps are removed, while VF-CsmA and GF-CsmA are forms where a V or G residue was added at the C terminal. The rationale behind comparing these residues is that although tCsmA works, the additional groups may affect the self-assembly process, and by adding another residue instead of the caps it is possible to make a comparison between capped and bare peptides without changing the molecular weight and length significantly.

For the tCsmA, two different modes of self-assembly are found. It forms filaments that are predominantly helical, and the formation of a para-crystalline sheet similar to the natural baseplate is a rare event. It can be observed after dialysis to the Tris buffer, which appears to provoke untwisting of the helical structure and formation of salt bridges between

antiparallel peptide strands. Interestingly, the capping appears to be essential for the self-assembly, since for the uncapped versions modulated self-assembly by dialysis is difficult.

3.2 Experimental section

3.2.1 Materials

Zn (II) Protoporphyrin IX (ZnPP) was purchased from Frontier Scientific. Variants of truncated CsmA were purchased from GL Biochem Ltd (98% purity). DMSO (Sigma Aldrich), monobasic dihydrogen phosphate (Sigma Aldrich), dibasic monohydrogen phosphate (Sigma Aldrich), HG, OG and 1-propanol (Sigma Aldrich), Amicon® Ultra Centrifugal Filters (Sigma Aldrich) and microdialysis vials (Pierce™ 96-well Microdialysis Plate, 3.5K MWCO, Thermo Fisher Scientific) were used for the constitution.

3.2.2 Equipment

The concentration of protein was measured with a Microvolume DS-11 Spectrophotometer (DeNovix). The UV-Vis spectra were measured using a UV-1700 Spectrophotometer (Shimadzu). Negative stain images were obtained with a JEM-1010 transmission electron microscope with a maximum output voltage up to 70 kV, equipped with an Olympus Megaview camera (JEOL Ltd.). The CD spectra were measured using a J-815 CD spectrometer (JASCO). The time-resolved fluorescence measurements were performed with a FluoTime 300 spectrometer (PicoQuant). Cryo-EM data were collected at 300 kV with a Titan Krios electron microscope (Thermo Fisher Scientific).

3.2.3 Methods

Constitution of the tCsmA-ZnPP complex was carried out in a 5:1 mixture of ZnPP (Frontier Scientific) and tCsmA dissolved in a pH 7.9 50 mM KPi buffer containing either 6M 1-propanol or 8% HG detergent (Sigma Aldrich). The ZnPP was added from a 200 mM DMSO (Sigma Aldrich) stock solution. The coordination and self-assembly proceeded in the microdialysis vial (Pierce™ 96-well Microdialysis Plate, 3.5K MWCO, Thermo Fisher Scientific) against a

4 times 1.4 mL KPi dialysis buffer at 4 °C in the dark. The first two and the last dialysis steps were for 2 hours, while for the third dialysis step the sample was incubated overnight. For the OG solution, dialysis was performed twice overnight. All other conditions except for the dialysis times were kept the same as for the procedure with 1-propanol or 8% HG detergent solution. After the last dialysis step, the samples were centrifuged for 15 minutes at 4 °C with 4,000 $\times$ *g* to remove remaining free CsmA and ZnPP precipitate. The dialysis conditions were modified with respect to pH, temperature and dialysis time tor the other truncated variants. Dialysis times of 1h, 4 h or overnight were used, and. the pH of the dialysis buffer was varied over a range of 6.1-7.9. Finally, different peptide to ZnPP molar ratios 2:1, 1:1, 1:2,..., 1:10 were used in addition to 1:5 for optimizing the protocol.

For Cryo-EM and negative staining TEM, the method was described in Chapter 2.

For the time-resolved fluorescence measurements, samples were prepared with 3.5 µM tCsmA-ZnPP complex in the KPi buffer or the Tris buffer. The excitation beam was 440 nm.

The binding of tCsmA and ZnPP was determined from the optical shift of the ZnPP using a UV-1700 Spectrophotometer (Shimadzu) as described in Chapter 2. The binding condition was optimized by varying the pH over a range of 6.1-7.9.

To assess the secondary structure of variants of truncated CsmA and the tCsmA-ZnPP complex, CD spectra were measured using a J-815 CD spectrometer (JASCO).

3.3 Results and discussion

3.3.1 Conditions for self-assembly of the tCsmA-ZnPP complex

As an amphipathic α-helical peptide, tCsmA contains a hydrophobic side that can be stabilized by the hydrophobic sides of neighboring peptides in a

packed assembly, and a hydrophilic side to associate with water to increase the solubility.[9] Apart from the amphipathic property, intermolecular interactions are also necessary to drive the peptides to form an ordered supramolecular structure.[10] The driving force can be hydrogen bonds, salt bridges, the effect of ligands and specific functional groups to form *e.g.* disulfide bridges or π-π stacking interactions.[11]

Table 3.1 Information of different truncated CsmA

Name	Sequence	Calculated pI	MW
F-CsmA	FTDILAAAGRIFEVMVEGHWETVGMLFDSLGKGTMRINRNAYG	5.65	4718
VF-CsmA	VFTDILAAAGRIFEVMVEGHWETVGMLFDSLGKGTMRINRNAYG	5.65	4817
GF-CsmA	GFTDILAAAGRIFEVMVEGHWETVGMLFDSLGKGTMRINRNAYG	5.65	4775
tCsmA	Ac-FTDILAAAGRIFEVMVEGHWETVGMLFDSLGKGTMRINRNAYG-NH_2	6.52	4759

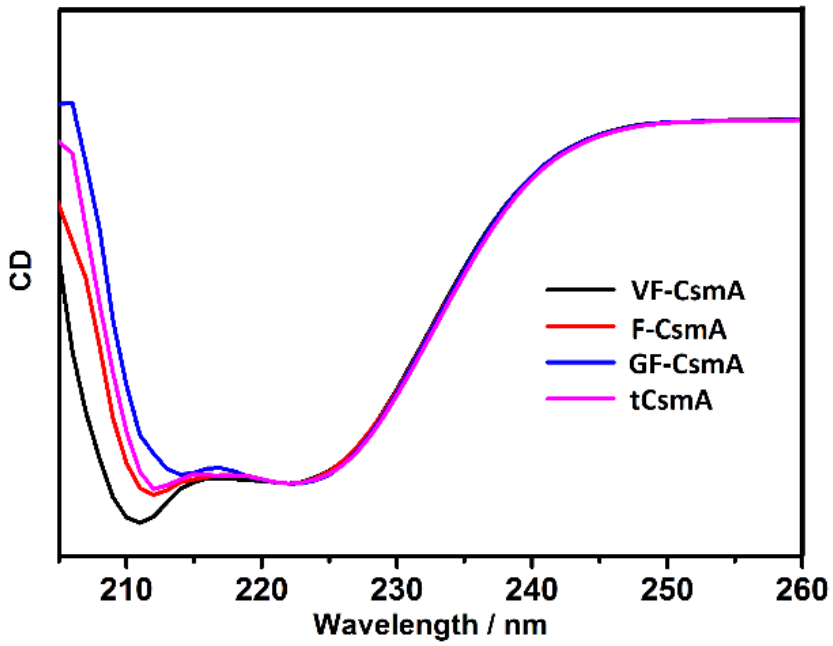

Figure 3.1 CD spectra for various truncated CsmA peptides dissolved in a propanol buffer.

To study the self-assembly behaviour, different truncated CsmA homologues were prepared (Table 3.1). tCsmA was prepared by N-terminal acetylation and C-terminal amidation to replace the flexible segments in the natural peptide. As was shown in Chapter 2, this leaves essential biological properties such as self-assembly and cofactor binding intact. As the CD spectra show, an α-helical structure was preserved for all variants studied, and in particular the CD spectra of tCsmA and F-CsmA virtually overlap

(Figure 3.1). This validates our hypothesis that the different truncations have little influence on the secondary structure. In Fig 3.2 UV-Vis spectra are shown, which shows whether the tCsmA and the ZnPP ligand coordinate to form an ordered assembly at different 6.1<pH<7.9. In contrast with the tCsmA, although these other peptides maintain the helical secondary structure of the natural system, little evidence for binding and complex formation is obtained, also when the pH, or the dialysis time and temperature are changed. The pI changes from pI=6.52 for the tCsmA to pI=5.65 for the other peptides.[12-13] When the pH > pI, a protein has a net negative charge and when the pH < pI, a protein has a net positive charge.[14] From pH 7.1 to pH 7.9 the other variants carry more significant negative charge than tCsmA. This may prohibit binding in the alkaline environment required for histidine coordination to the ZnPP to proceed. As the net charge of a protein directly influences many of its properties, such as solubility, assembly and crystallization, these other factors can be important as well.[15-16]

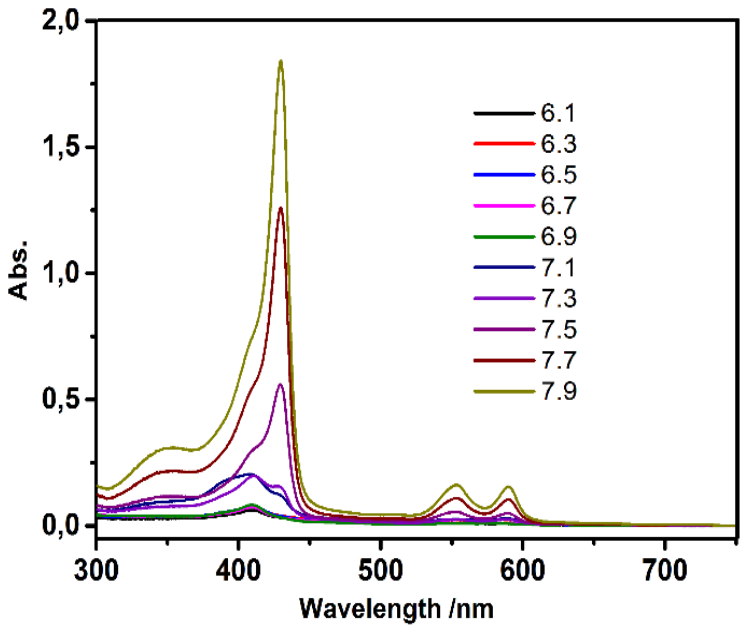

Figure 3.2 UV-vis spectra for the pH dependent constitution of tCsmA-ZnPP.

On the other hand, the pH of the dialysis buffer is important for the binding of ligand. As Figure 3.2 shows, when the buffer became basic pH>7 the binding could occur, and the binding became more efficient with the higher pH of the dialysis buffer, up to pH 7.9. This confirms that the basic

nitrogen atom in the imidazole of histidine with a lone electron pair can coordinate to metallic cations like the Zn^{2+} of ZnPP when the pH becomes basic.[17]

Because tCsmA and ZnPP both are insoluble in aqueous solution before self-assembly, the choice of solvent also influences the constitution. Detergents are used to solubilize tCsmA and ZnPP and keep the original secondary structure.[18] To avoid the interruption of binding by the micelles of detergents, the solution has to be diluted until the concentration of detergents is below the CMC.[19] This eliminates the micelles to promote the binding of tCsmA and ZnPP.[19] When the complex is prepared in this way, the complex cannot be concentrated since micelles will re-form during the concentration when using centrifugal filters. However, the detergents can be removed by dialysis. In addition, the unbound ZnPP and tCsmA precipitate upon removal of the detergent. As a result, according the UV data we are able to obtain a very pure complex when using the dialysis method for the constitution (Figure. 3.2).

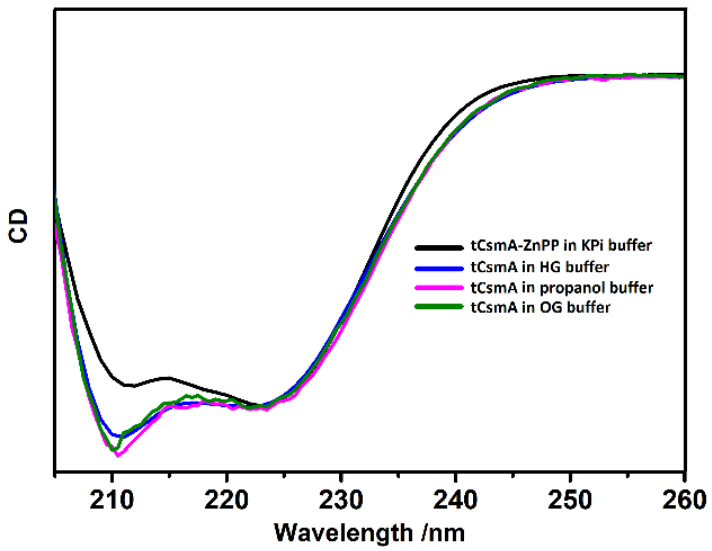

Figure 3.3 CD spectra for the tCsmA in different solvents and for the tCsmA-ZnPP construct in the KPi buffer.

The detergents with low CMC value are difficult to remove by dialysis, since the micelles are too large to pass through the membrane. Therefore, detergents with high CMC such as HG and OG are recommended. 1-propanol also increases the solubility of tCsmA, but with no risk of micelles.

The CD spectra of tCsmA in the propanol buffer and the detergent buffer overlap, and both show the characteristic shape for an α-helical structure (Figure 3.3). Thus, the 1-propanol and detergents keep the natural state of the tCsmA for ligand coordination.[20] However, although the detergents and 1-propanol cover the hydrophobic side to increase the solubility of tCsmA, the tCsmA peptides still randomly aggregate together. The solubility is limited to about 130 μM. The histidine coordination position is located at the hydrophobic side, and the detergents and 1-propanol have to be dialyzed out to expose the histidine for the coordination of ZnPP. For the HG and 1-propanol buffer, the complex is formed during the first 2 h of dialysis. However, the OG detergent with lower CMC is much slower to be dialyzed out of the membrane, and the formation of complex occurs after a 2 times dialysis overnight. The experiments indicate that the tCsmA peptides aggregate easily. Only after binding with ZnPP the peptides start to form large homogeneous filaments. Therefore the ZnPP also plays an important role in the self-assembly. The CD spectra in Figure 3.3 also show the change of tCsmA after the binding. The α-helical structure was still maintained after the binding, but the intensity at 211 nm and 216 nm increased. This is probably caused by the change in the loop between two helical regions of tCsmA. After self-assembly, the loop of peptides was aligned with two helical regions to form a straight α-helical peptide.

3.3.2 The helical structure of the self-assembly

The tCsmA-ZnPP complex is able to self-assemble to form 7_2 helical filaments after dialysis in the KPi buffer (cf. Chapter 2). The length of most filaments is a few micrometers (Figure 3.4A). Under negative stain TEM conditions, the images show strands or bundles (Figure 3.4B). The diameter of most bundles is around 10-20 nm, and the diameter of a single filament is about 5 nm. Self-assembly over extended time periods of 1 month leads to a very limited solubility, around 250 μM, which is attributed to the formation of larger aggregates over time. When the solution of the complex was centrifuged at 50,000 rpm, nearly all filaments precipitate in 30 minutes. On the other hand, the complex can be precipitated without centrifugation when the concentration of the KPi buffer is increased to 1 M. Both precipitates still maintain the same optical absorption characteristics when the sample is re-dissolved. The details of the helical structure are presented in Chapter 4.

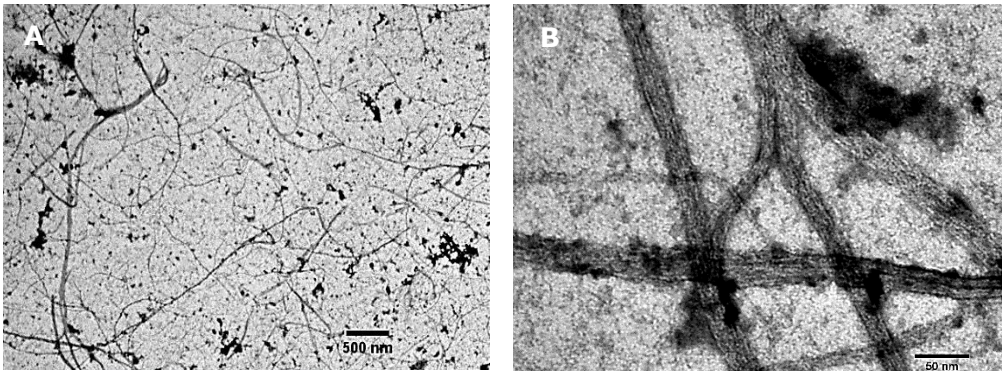

Figure 3.4 (A), (B) TEM image of the tCsmA-ZnPP complex in the KPi buffer.

3.3.3 The para-crystalline structure of the self-assembly

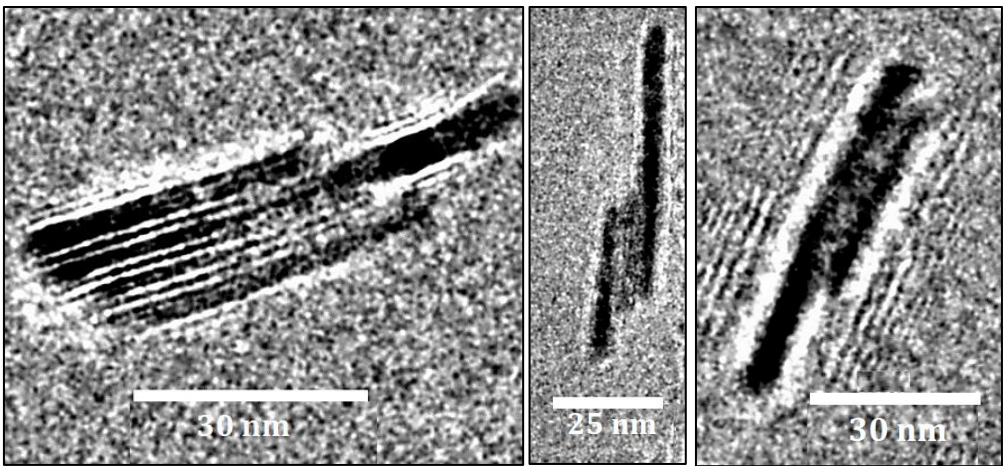

Figure 3.5 The cryo-EM images of transitional particles in the Tris buffer.

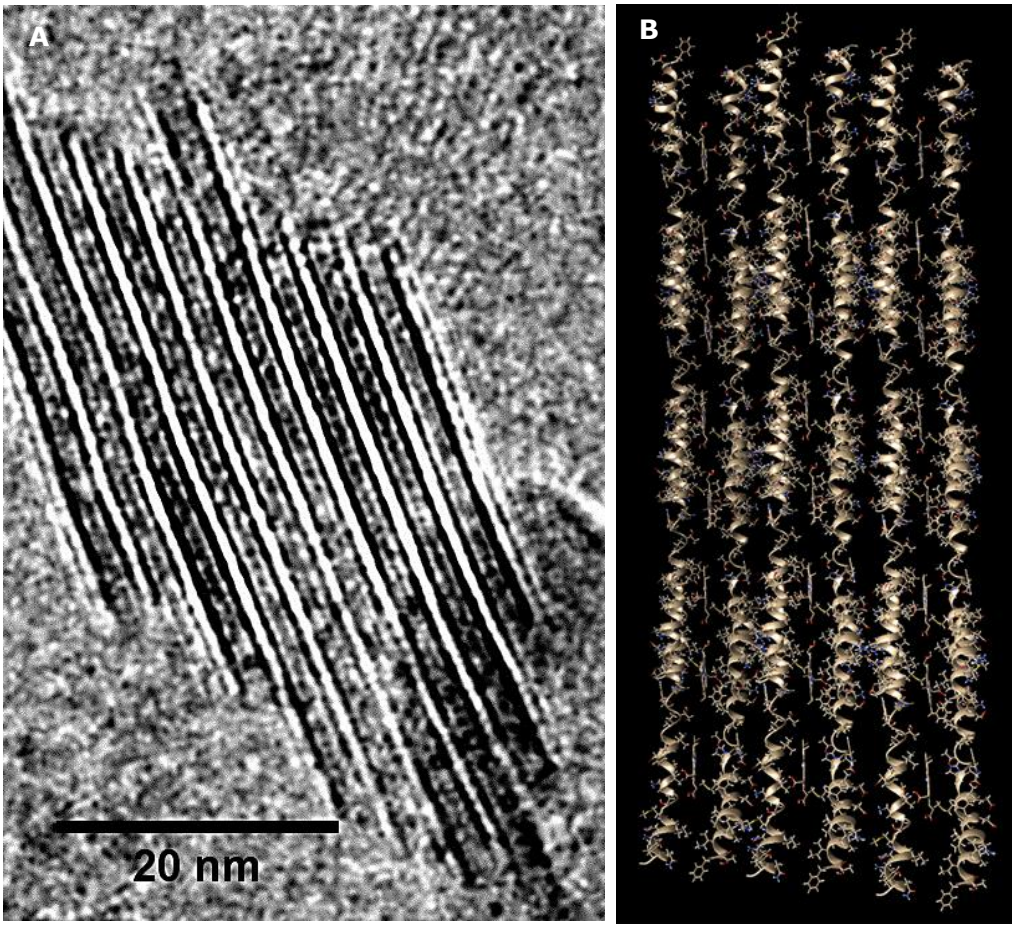

Figure 3.6 (A) Cryo-EM image of a para-crystalline self-assembly of the tCsmA-ZnPP complex in the Tris buffer. (B) The simulated para-crystalline self-assembly of the tCsmA-ZnPP complex in the Tris buffer.

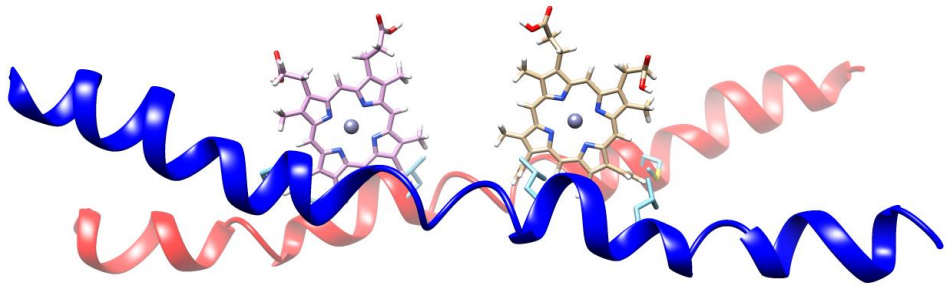

Figure 3.7 The dimeric unit of the para-crystalline baseplate

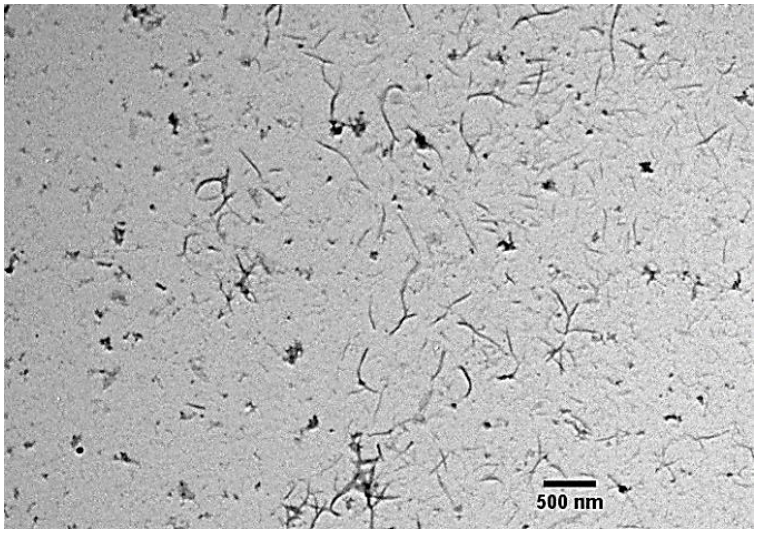

Figure 3.8 Negative staining TEM image of the tCsmA-ZnPP complex in the Tris buffer.

Tris buffer cannot be used as the dialysis buffer for the complex constitution. However, when the complex in the KPi buffer is dialyzed to the Tris buffer, the complex remains intact. Most filaments break up into smaller pieces during the dialysis, but without breaking down the complex (Figure 3.8).

In selected images, planar structures are observed that resemble the natural CsmA baseplate antenna. We attribute these planar structures to the untwisting of helical filaments upon changing the buffer (Figure 3.5). In the helix, the ZnPP interact to form a tetramer (Chapter 2), while in the planar form the ZnPP forms extended linear arrays of dimeric ZnPP in between two tCsmA strands (Figure 3.6). It is tempting to conclude that, similar to the natural baseplate, salt bridges can stabilize the planar form of the tCsmA-ZnPP complex. The baseplate structure is provoked by the untwisting of the helical structure and the formation of salt bridges between antiparallel peptide strands with arrays of dimeric ZnPP coordinated to the histidyl between the strands. The ZnPP shows a vertical orientation between tCsmA strands (Figure 3.7).

As Figure 3.6A shows, the distance between strands is about 31.3 Å, which is the same as for the natural baseplate. According to the EM data, the ZnPP is embedded in the middle of the strands and is oriented perpendicular to the plane of the assembly. Probably the hydrophobic side of the self-assembly is turned nearly 90° relative to the helical form to interact with the adjacent

complex in the other strand directly. As a result, the dimeric ZnPP cannot interact with the ZnPP motifs in neighboring strands. Thus, in the crystalline structure, the ZnPP forms a dimeric unit rather than a tetrameric unit as Figure 3.7 shows.

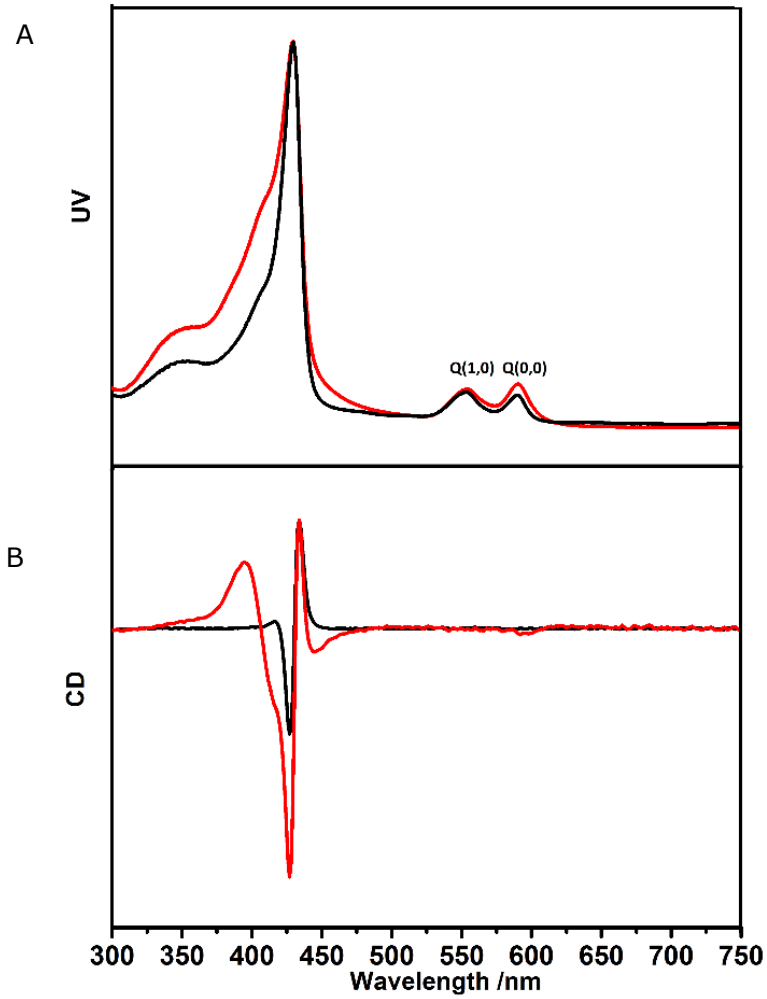

Figure 3.9 UV-vis and corresponding CD spectra of the tCsmA-ZnPP complex in the KPi buffer (black trace) and the Tris buffer (red trace) respectively.

Figure 3.9 indicates the conformational changes that are observed in optical spectroscopy for the two sample species. The UV-Vis spectrum of the complex in the Tris buffer shows a broad peak at 430 nm which indicates less homogeneity in the Tris buffer (Figure 3.9A). Moreover, the UV-Vis absorption of Q(0,0) becomes higher than for the Q(1,0). This indicates that the ZnPP may be less planar in the Tris buffer relative to the KPi buffer.[21-22]

This is corroborated by the CD response of the complex. The CD response of the complex in Tris buffer is asymmetric, which contrasts with the symmetric spectrum in the KPi buffer due to the tetrameric ZnPP in the 7_2 helix (Figure 3.9B and Chapter 2). However, the CD response of the Q bands in the Tris buffer is quenched, similar to the helical form. This suggests reorientation of the molecule going from the tetramers in the helical form to the linear arrays in the planar form into a configuration to offset any dipole-dipole interactions that could give rise to a CD response.[23-24]

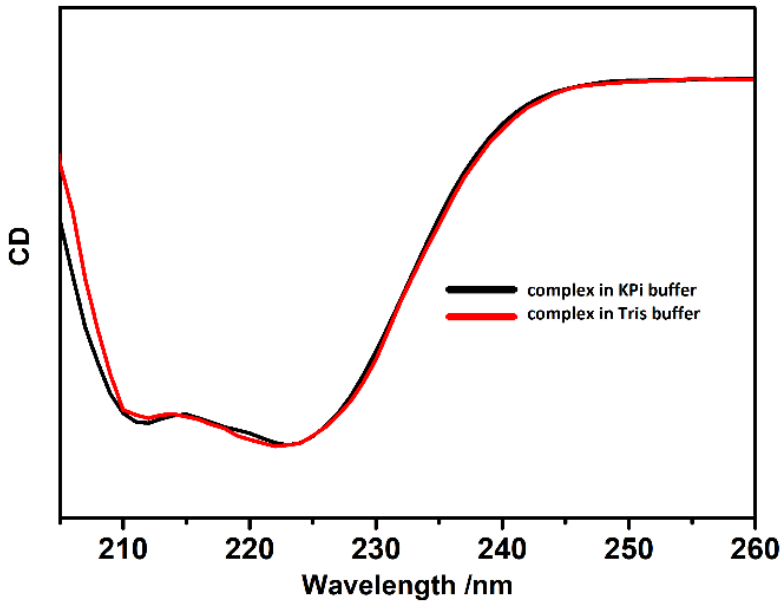

Figure 3.10 CD spectra of the tCsmA-ZnPP complex in the KPi buffer (black trace) and the Tris buffer (red trace) respectively.

As Figure 3.9B shows, the intensity ratio of the negative and positive CD responses for the ZnPP is more than 2, which indicates structural rearrangement at the level of the complex when it is transferred to another buffer. However, in the CD data in Figure 3.10, there is considerable spectral overlap, which indicates that overall the tCsmA helical peptide has little conformational change of secondary structure on the peptide level upon buffer change.

Table 3.2 Fitted Time constants of Fluorescence Transients of the tCsmA-ZnPP complex in the Tris buffer under a 440 nm excitation.

Buffer	594 nm Lifetime, ns				650 nm Lifetime, ns			
Lifetime	τ_1	τ_2	τ_3	$\tau_{average}$	τ_1	τ_2	τ_3	$\tau_{average}$
Tris buffer	2.64 (3%)	1.21 (45%)	0.4 (52%)	0.84	5.15 (2.4%)	1.36 (44%)	0.45 (53.6%)	0.97

Finally, for the ZnPP in the Tris buffer the photochemical properties are very similar to the system in the KPi buffer (Table 3.2 and Chapter 2 Table 2.3). The complexes in the Tris and the KPi buffer both have 3 similar lifetimes at the same emission peaks at 594 nm and 650 nm. Apparently the loss of symmetry in the Tris buffer has little effect on the decay characteristics.

3.4 Conclusion

At near neutral pH 7.1-7.9, binding of tCsmA to ZnPP is observed with dialysis in the KPi buffer. In addition, a high pH of the dialysis buffer is important for the self-assembly of tCsmA and ZnPP. The net charge of the protein was implied to be important for the self-assembly. Hence N-terminal acetylation and C-terminal amidation promote self-assembly. While the principle structure of self-assembly is a 7_2 helix, the tCsmA-ZnPP complex is able to form another type of ordered chiral matrix in the Tris buffer that mimics the baseplate array in the natural system and appears stabilised by hydrophobic effects, salt bridges, and dipole-dipole interactions of chromophores. It is tempting to conclude that the para-crystalline baseplate structure is formed by the untwisting of the 7_2 helix and the reorientation of the peptide strands to accommodate salt bridges between strands.

3.5 References

1. Frigaard, N.-U.; Bryant, D. A., Chlorosomes: Antenna Organelles in Photosynthetic Green Bacteria. In *Complex Intracellular Structures in Prokaryotes*, Shively, J. M., Ed. Springer Berlin Heidelberg: Berlin, Heidelberg, 2006; pp 79-114.
2. Li, H.; Frigaard, N.-U.; Bryant, D. A., *Biochemistry* **2006,** *45* (30), 9095-9103.
3. Pedersen, M. Ø.; Underhaug, J.; Dittmer, J.; Miller, M.; Nielsen, N. C., *FEBS Letters* **2008,** *582* (19), 2869-2874.
4. Bryant, D. A.; Vassilieva, E. V.; Frigaard, N.-U.; Li, H., *Biochemistry* **2002,** *41* (48), 14403-14411.
5. Zobova, A.; Taisova, A.; Lukashev, E.; Fedorova, N.; Baratova, L.; Fetisova, Z., *Journal of Biophysics* **2011,** *2011*.
6. Kulminskaya, N. V.; Pedersen, M. Ø.; Bjerring, M.; Underhaug, J.; Miller, M.; Frigaard, N. U.; Nielsen, J. T.; Nielsen, N. C., *Angewandte Chemie International Edition* **2012,** *51* (28), 6891-6895.
7. Nielsen, J. T.; Kulminskaya, N. V.; Bjerring, M.; Linnanto, J. M.; Rätsep, M.; Pedersen, M. Ø.; Lambrev, P. H.; Dorogi, M.; Garab, G.; Thomsen, K., *Nature communications* **2016,** *7*, 12454.
8. Andrew Staehelin, L.; Golecki, J. R.; Drews, G., *Biochimica et Biophysica Acta (BBA) - Bioenergetics* **1980,** *589* (1), 30-45.
9. Azzarito, V.; Long, K.; Murphy, N. S.; Wilson, A. J., *Nature Chemistry* **2013,** *5*, 161.
10. Hu, K.; Jiang, Y.; Xiong, W.; Li, H.; Zhang, P.-Y.; Yin, F.; Zhang, Q.; Geng, H.; Jiang, F.; Li, Z.; Wang, X.; Li, Z., *Science Advances* **2018,** *4* (5), eaar5907.
11. Bai, Y.; Luo, Q.; Liu, J., *Chemical Society Reviews* **2016,** *45* (10), 2756-2767.
12. Bjellqvist, B.; Hughes, G. J.; Pasquali, C.; Paquet, N.; Ravier, F.; Sanchez, J.-C.; Frutiger, S.; Hochstrasser, D., *ELECTROPHORESIS* **1993,** *14* (1), 1023-1031.
13. Gauci, S.; van Breukelen, B.; Lemeer, S. M.; Krijgsveld, J.; Heck, A. J. R., *PROTEOMICS* **2008,** *8* (23‐24), 4898-4906.
14. Kozlowski, L. P., *Nucleic acids research* **2017,** *45* (D1), D1112-D1116.
15. Gitlin, I.; Carbeck, J. D.; Whitesides, G. M., *Angewandte Chemie International Edition* **2006,** *45* (19), 3022-3060.
16. Shaw, K. L.; Grimsley, G. R.; Yakovlev, G. I.; Makarov, A. A.; Pace, C. N., *Protein science : a publication of the Protein Society* **2001,** *10* (6), 1206-1215.
17. Liao, S.-M.; Du, Q.-S.; Meng, J.-Z.; Pang, Z.-W.; Huang, R.-B., *Chemistry Central journal* **2013,** *7* (1), 44-44.
18. Nagarajan, R.; Ganesh, K., *Macromolecules* **1989,** *22* (11), 4312-4325.
19. Pedersen, M. Ø.; Pham, L.; Steensgaard, D. B.; Miller, M., *Biochemistry* **2008,** *47* (5), 1435-1441.
20. Singh, S. M.; Sharma, A.; Upadhyay, A. K.; Singh, A.; Garg, L. C.; Panda, A. K., *Protein expression and purification* **2012,** *81* (1), 75-82.
21. Milgrom, L. R.; Warren, M. J., **1997**.

22. Giovannetti, R., The use of spectrophotometry UV-Vis for the study of porphyrins. In *Macro to nano spectroscopy*, IntechOpen: 2012.
23. Harada, N.; Nakanishi, K., *Accounts of Chemical Research* **1972,** *5* (8), 257-263.
24. Pescitelli, G.; Gabriel, S.; Wang, Y.; Fleischhauer, J.; Woody, R. W.; Berova, N., *Journal of the American Chemical Society* **2003,** *125* (25), 7613-7628.